

Enhancing Quantum Otto Engine Performance in Generalized External Potential on Bose-Einstein Condensation Regime

Zahara Zettira¹, Ade Fahriza¹, Zulfi Abdullah¹, and Trengginas E P Sutantyo^{1*}

¹*Theoretical Physics Laboratory, Department of Physics,
Faculty of Mathematics and Natural Science, Andalas University, Indonesia*

(Dated: March 25, 2024)

We examine a quantum Otto engine using both Bose-Einstein Condensation (BEC) and normal Bose gas as working medium trapped in generalized external potential. We treated the engine quasi-statically and endoreversibly. Since the expansion and compression in both quasi-static and endoreversible take place isentropic, the expression of efficiency is similar. However, the power output in the quasi-static cycle is zero due to infinite and long stroke time. In contrast, with an endoreversible cycle, thermalization with two reservoirs takes place at a finite time. We use Fourier's law in conduction to formulate the relation between temperature of medium and reservoir, making work depend on heating and cooling stroke time. Moreover, we maximized the power with respect to compression ratio κ to obtain efficiency at maximum power (EMP). We found that EMP is significantly higher when using BEC as a working medium, meanwhile EMP with normal Bose gas is just Curzon-Ahlborn efficiency. We also investigate the effect of thermal contact time τ with hot (τ_h) and cold (τ_l) reservoir on EMP. We found that when complete thermalization, $\tau_h = \tau_l$, stroke time occurs, there are no significant differences. Nevertheless, while incomplete thermalization arise, by adjusting various cooling and heating stroke time, provides a significant result on EMP, which is much higher at $\tau_h < \tau_l$ stroke time whilst lower at $\tau_h > \tau_l$ stroke time. We conclude this incomplete thermalization leads to the condition where residual coherence emerges which enhances the EMP of the engine.

I. INTRODUCTION

Nowadays, quantum science significantly influences the development of classical physics theory, unexceptionable thermodynamics, which has recently been known as quantum thermodynamics [1] or nano thermodynamics [2]. Since the discovery of quantum science, nano thermodynamics has emerged rapidly [3–10] and being fundamental for future advanced technologies [11]; quantum information, high precision sensors, and quantum heat engine (QHE). Started by the pioneer of QHE [12] until recent development [11, 13]; this revolution is a bridge to the breakthrough implementation of nano heat engines. Over the last two decades, research on quantum heat engines has opened up the horizons of their benefits. [14]. The motivation is to realize the QHE as close as possible to the practical world as a worthwhile device.

Quantum Heat Engine (QHE) is a device that utilizes quantum matter or particles as its working medium in order to convert heat into work [15]. In fact, the QHE also operates using a cycle that resembles classical thermodynamics, such as the Otto [16–20], Lenoir [21–26], Diesel [27, 28], and Carnot [20, 29–34] cycles. Nevertheless, the physical quantities in the quantum thermodynamic cycle are different from the classical thermodynamic cycle; this is the underlying reason that the efficiency of a quantum heat engine is ably outperformed the most efficient classical heat engine, the Carnot Engine [35]. In a certain state, the work produced by QHE exceeds the maximum value of a heat engine which operates classically [36–38].

A classical heat engine that operates with a reversible cycle produces the highest efficiency, e.g., classical Carnot engine. However, the Carnot engine operates via a quasistatic process that lasts long and produces zero power output, making it impossible to realize. Curzon and Ahlborn [39] applied an endoreversible approach, in which the process is accelerated, and the power output produced by the engine is finite. Although the efficiency η_{CA} is lower than the efficiency of a quasistatic Carnot engine η_C , an endoreversible Carnot engine is more realistic and possible to realize.

Recently, many heat engine models proposed to investigate the endoreversible cycle because it is more realistic to implement [36, 40–46], even those endoreversible heat engines have an efficiency that exceeds Curzon-Ahlborn limit [39]. The endoreversible heat engine model uses a variety of mediums such as classical gas [47, 48], single ion [36, 40, 44], or even quantum matter in the form of fermions [49] and bosons [43, 50–52].

Interestingly, boson as a working medium produces greater efficiency than fermion achieves [43], due to the advantages of symmetry possessed by boson that fermion does not. This is what underlies this research to examine the role of boson as a working medium, especially in the Bose-Einstein Condensation (BEC) regime, which is even claimed to be able to provide better performance than ordinary boson gas [42]. The use of BEC as a heat engine working medium is being intensively investigated [42, 50–53]. When the bosonic atoms gas is cooled below a certain critical temperature T_c , such that most of the atoms are condensed in the lowest quantum state, experience a phase transition into BEC regime [54, 55]. BEC is a quantum phenomenon that can be realized on sev-

* trengginasekaputra@sci.unand.ac.id

eral vapors, i.e., rubidium [56], sodium [57], and lithium [58, 59]. Moreover, recently BEC can be observed in a 3D potential box [60].

In this study, we examine the quantum Otto engine using the advantage of the BEC's thermodynamic properties as a working medium under the influence of a 3D generalized external trapping potential. We modify that typical potential [61] in order to investigate performance in other circumstances, especially considering the possibilities of the cycles that can exploit external trapping potential as a bridge to extending the analysis to the nonequilibrium regime [42]. Besides, with that potential, the engine aims to obtain better performance, considering for $n \rightarrow \infty$, i.e., box potential, provides lower heat capacity (c_V) than for $n = 2$, i.e., harmonic potential [61]. This will affect the efficiency of the Otto engine $\eta(c_V)$, with box potential achieving higher efficiency than harmonic potential. In addition, we compare the performance of quantum Otto engine from work and efficiency both in condensed and non-condensed phase. Apart from that, we investigate the engine performance from efficiency at maximum power (EMP) by maximizing the power output to the compression ratio parameter. Lastly, we also explore the engine performance by varying thermalization time during the cycles, which at a specific value boosts the EMP significantly.

II. THERMODYNAMIC PROPERTIES OF BEC IN GENERALIZED EXTERNAL POTENTIAL

We consider N number of particles in an ideal Bose gas to be equally distributed in a certain energy level. This energy level is determined by the Hamiltonian worked in the aforementioned particles. In this study, we define ideal Bose gas in generalized external trapping potential as formulated below

$$V(\mathbf{r}) = \varepsilon_0 \left(\left| \frac{x}{a} \right|^p + \left| \frac{y}{a} \right|^q + \left| \frac{z}{a} \right|^l \right) \quad (1)$$

where x , y , and z are coordinate of the particles' positions in space, ε_0 is a constant in energy dimension, and a is radius of the potential. Here, we set $p = q = l = n$, so for certain n numbers, the potential has shape as Figure 1.

The density of state for distributed particles in potential from Equation 1 is given by [61]

$$\rho(\varepsilon) = \left[\frac{2\pi(2m)^{\frac{3}{2}}}{h^3} \right] \frac{a^3}{\varepsilon_0^{\frac{3}{n}}} \varepsilon^\lambda F(n, n, n) \quad (2)$$

where $\lambda = \frac{3}{n} + \frac{1}{2}$ and $F(n, n, n)$ is defined as below

$$F(n, n, n) = \left[\int_{-1}^1 (1 - X^n)^{\frac{1}{2} + \frac{2}{n}} dX \right] \times \left[\int_{-1}^1 (1 - X^n)^{\frac{1}{2} + \frac{1}{n}} dX \right] \times \left[\int_{-1}^1 (1 - X^n)^{\frac{1}{2}} dX \right]. \quad (3)$$

Grand potential for the boson particle system is given by [62]

$$\Omega = k_B T \sum_i \ln(1 - ze^{-\beta \varepsilon_i}) \quad (4)$$

which $z = e^{\frac{\mu}{k_B T}}$ is the fugacity. Since in BEC cases, the big fraction of bosons are condensed into ground state energy, we can consider $k_B T \gg \varepsilon_{i+1} - \varepsilon_i$. Therefore, the system can be defined as a continuous state plus a discrete ground state. By substituting Equation 2 to Equation 4, we obtain

$$\begin{aligned} \Omega &= A k_B T a^3 \int_0^\infty \varepsilon^{\frac{3}{n} + \frac{1}{2}} \ln(1 - ze^{-\varepsilon \beta}) d\varepsilon \\ &= -A' a^3 (k_B T)^{\frac{3}{n} + \frac{5}{2}} g_{\frac{3}{n} + \frac{5}{2}}(z) \end{aligned} \quad (5)$$

with $A = \left[\frac{2\pi(2m)^{\frac{3}{2}}}{h^3} \right] \frac{F(n, n, n)}{\varepsilon_0^{\frac{3}{n}}}$ and $A' = \frac{1}{\frac{3}{n} + \frac{5}{2}} \Gamma\left(\frac{3}{n} + \frac{5}{2}\right) A$ which are constants and $b = \frac{3}{n} + \frac{5}{2}$ is used to shorten the notations. Furthermore, $g_{\frac{3}{n} + \frac{5}{2}}(z)$ is the related Bose function which is defined in the following equation [62]

$$g_v(z) = \frac{1}{\Gamma(v)} \int_0^\infty dx \frac{1}{z^{-1} e^x - 1} \quad (6)$$

Bose function can also be defined as a series that is similar to the Zeta function series,

$$g_v(z) = \sum_{n=1}^{\infty} \frac{z^n}{n^v} \quad (7)$$

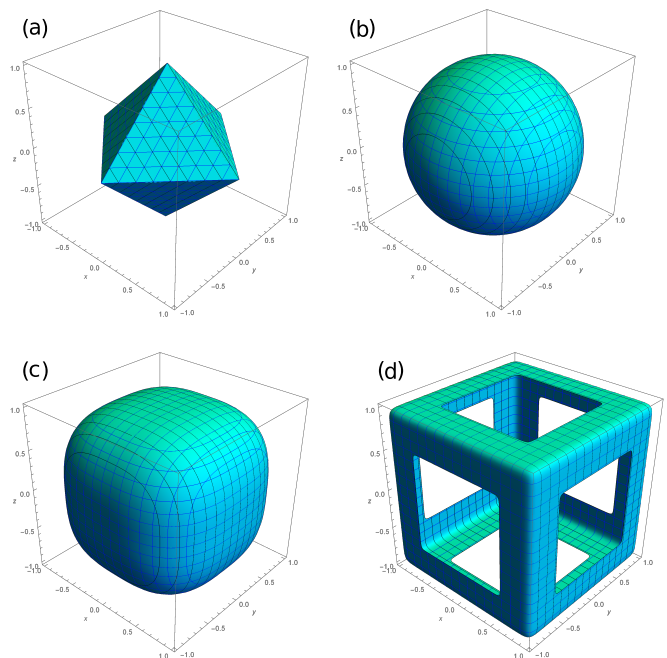


FIG. 1. Illustration of external potential with (a) $n = 1$, (b) $n = 2$, (c) $n = 3$, and (d) $n \rightarrow \infty$ respectively.

and can also be expressed in the following recursion relation,

$$g_{v-1}(z) = \frac{\partial}{\partial \ln(z)} g_v(z) \quad (8)$$

Based on $\Omega = U - TS - \mu N$ relation [62], we can derived N that is the number of excited atom at temperature T

$$N = - \left(\frac{\partial \Omega}{\partial \mu} \right)_{T,a} = A' a^3 (k_B T)^b g_b(z) \quad (9)$$

BEC occurs when μ increases monotonously until the value approaches the energy at ground state (ε_0). If $\varepsilon_0 = 0$ [63], then BEC occurs at $\mu = 0$ or $z = 1$ so that we can derive the critical temperature, the temperature at the phase transition, as

$$T_c = \left[\frac{N}{A' a^3 \zeta(b)} \right]^{\frac{1}{b}} \frac{1}{k_B} \quad (10)$$

The entropy S and the internal energy U of the BEC can be derived respectively, as follow

$$S = - \left(\frac{\partial \Omega}{\partial T} \right)_{T,a,\mu} = \begin{cases} A' a^3 k_B (k_B T)^b [(b+1)g_{b+1}(1)] & T \leq T_c \\ A' a^3 k_B (k_B T)^b [(b+1)g_{b+1}(z) - \ln z g_b(z)] & T \geq T_c \end{cases} \quad (11)$$

and

$$U = \Omega + TS + \mu N = \begin{cases} (b)A'a^3(k_B T)^{b+1}g_{b+1}(1) & T \leq T_c \\ (b)A'a^3(k_B T)^{b+1}g_{b+1}(z) & T \geq T_c \end{cases} \quad (12)$$

III. ENDOREVERSIBLE OTTO CYCLE

The main principle of endoreversible thermodynamics is local equilibrium. The transformation of working medium during isentropic stroke takes place slowly so that the working medium is always able to reach equilibrium. However, because the cycle time is finite, the working medium does not have time to reach equilibrium with the reservoir. So, from the reservoir point of view, the process is irreversible, but from the working medium point of view itself, the process is reversible [64].

An ideal Otto cycle consists of four strokes: isentropic compression (stroke 1-2), isochoric heating (stroke 2-3), isentropic expansion (stroke 3-4), and isochoric cooling (stroke 4-1) [65], as shown in Figure 2. By varying a as a parameter shows potential radius, it means we variate the external potential for the system which also means there is a change in order of the energy at said system until the system is excited. On the other hand, imbuing thermal energy into the system can also cause excitation in the system. The energy transfer of the external field and the thermal energy are arranged in such a way that the Otto cycle is relevant to the classical Otto cycle.

During isochoric heating stroke, external field remains constant at a_l so as the volume and the system make contact with the hot reservoir, the heat flows into the system. Based on the first law of Thermodynamic, the amount of heat transferred is

$$\Delta Q_{in} = U(T_3, a_l) - U(T_2, a_l) \quad (13)$$

Heat transfer during heating stroke, the system obeys the

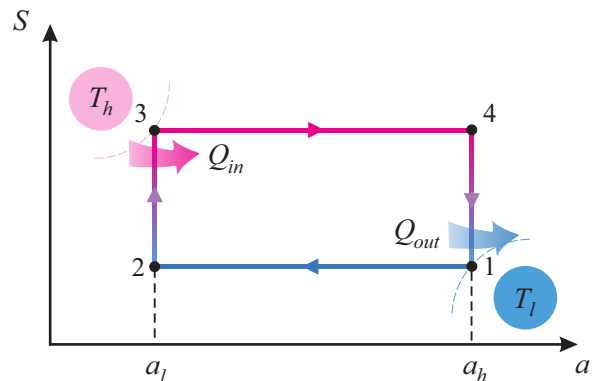


FIG. 2. Otto cycle diagram for Entropy S vs. external field a which heat exchange occurs only between 4-1 and 2-3 strokes due to isolation of isentropic conditions through 1-2 and 3-4 strokes.

Fourier heat conduction law as given

$$\frac{dT}{dt} = -\alpha_h (T - T_h) \quad (14)$$

where α_h is a constant that depends on thermal conductivity and thermal capacity of the medium during heating stroke. The boundary conditions at the beginning and the end of isochoric stroke are written as

$$T(0) = T_2 \text{ and } T(\tau_h) = T_3, \text{ where } T_2 < T_3 \leq T_h \quad (15)$$

with solution

$$T_3 - T_h = (T_2 - T_h)e^{-\alpha_h \tau_h} \quad (16)$$

when a time limit of heating stroke goes to infinity, $\tau_h \rightarrow \infty$, $T_3 = T_h$ and it becomes the quasi-static condition.

During isentropic expansion stroke, external field is varied from a_l to a_h which also means the volume of the system is changed from V_l to V_h . However, the system is unattached from the reservoir so that there is no heat exchange within the system ($\Delta Q = 0$). From the First Law of Thermodynamics, we get

$$W_{exp} = U(T_4, a_h) - U(T_3, a_l) \quad (17)$$

After the volume reach V_h , the system is back interconnected to the cold reservoir. During this stroke, the external field remains constant at a_h . Similar to the isochoric heating stroke, the ejected heat is the internal energy difference from stroke 3 to 2,

$$\Delta Q_{out} = U(T_1, a_h) - U(T_4, a_h) \quad (18)$$

Heat transfer process during cooling stroke which also obey the Fourier heat conduction law as below

$$\frac{dT}{dt} = -\alpha_l (T - T_l) \quad (19)$$

where α_l is a constant of thermal conductivity and thermal capacity of the medium during cooling stroke. This isochoric stroke has boundary conditions as

$$T(0) = T_4 \text{ and } T(\tau_l) = T_1, \text{ where } T_4 > T_1 \geq T_l \quad (20)$$

with solution

$$T_1 - T_l = (T_4 - T_l)e^{-\alpha_l \tau_l} \quad (21)$$

when quasi-static condition is achieved while cooling stroke time reaches the limit to infinity, $\tau_l \rightarrow \infty$, in other words, $T_1 = T_l$.

Furthermore, the system is re-disconnected from the reservoir and the field is varied a_h to a_l to fulfill isentropic conditions. As there is no heat transfer within the system, then the work during compressing stroke is given by

$$W_{comp} = U(T_2, a_l) - U(T_1, a_h) \quad (22)$$

Unlike the quasi-static Otto cycle, in which the four strokes are reversible, in the endoreversible Otto cycle, 2 strokes are irreversible and 2 strokes are reversible. Irreversibility occurs when the working medium comes into contact with the reservoir during isochoric stroke, which causes leaking during the heat transfer [66]. On the other hand, during isentropic strokes, there is no heat leaking occurs due to the system being isolated to external energy [66]. This idea has been demonstrated in recent studies. [36, 42, 45, 67]

Next, we determine the thermal efficiency by comparing the total work done in a cycle with the heat in

$$\eta = -\frac{W_{exp} + W_{comp}}{Q_{in}} \quad (23)$$

whilst the power output is determined by the total work done and the time for one cycle

$$P = -\frac{W_{exp} + W_{comp}}{\gamma \tau_h + \tau_l} \quad (24)$$

with γ is a multiplier constant that refers to the total time for one cycle, including the time throughout isentropic strokes.

To eliminate T_1, T_2, T_3 , and T_4 into controllable parameters (T_h, T_l), both Equation 17 and 22 are not enough so that another two equations are needed. During isentropic strokes, the entropy and fugacity are constant [36, 42] so based on Equation 11, within isentropic strokes, we got the relation of temperature as

$$T_2 = \kappa^{-\frac{1}{b}} T_1 \text{ and } T_4 = \kappa^{\frac{1}{b}} T_3 \quad (25)$$

which $\kappa = \left(\frac{a_l}{a_h}\right)^3$ is the ratio of volume compression.

IV. RESULT AND DISCUSSION

A. Quasi-static Performance

By using Equation 11, we obtain the critical temperature for $n = 1, 2, 3$ and $n \rightarrow \infty$, as shown in table 1 that T_c decreases as n increases. T_c for $n = 2$ is the same as Myers et al. obtained in their research [42] and other related data have also been adjusted according to reference [68]. This decrease in T_c is related to the volume of each potential as shown in Figure 1, where volume is proportional to n . Thus at the same number of particles N , potential with small V , the density of atoms is greater than the potential with large V . This is consistent with the results obtained by [69] that an increase in density of atoms causes an increase in T_c as well, so that at $n \rightarrow \infty$ the gas becomes less dense so T_c is also small.

TABLE I. Thermodynamics property of BEC using potential $n = 1, 2, 3$ and $n \rightarrow \infty$ with 60.000 bosons (Rubidium-87) and $a = 1$ mm

n	$F(n, n, n)$	b	T_c (nK)	$C_v(T_c^-)/Nk_B$	$C_p(T_c^-)/Nk_B$
1	13.78	9/2	280.39	24.06	29.41
2	2.46	3	41.28	10.82	14.40
3	7.83	5/2	6.05	7.34	10.28
∞	8	3/2	0.00722	1.92	3.20

In the quasi-static cycle all four-stroke is reversible, as consequences of internal friction due to expansion and compression during isentropic stroke are negligible. Since thermal contact within medium and reservoir last for long time, so we get from Equation 16 and 21 $T_3 = T_h$ and $T_1 = T_l$. For the cycle in quasi-static regime, we present the result in Figure 3 and 4. Figure 3 represent the numerical solutions of quasi-static Otto cycle which operated in non-condensed phase or just normal bose gas that

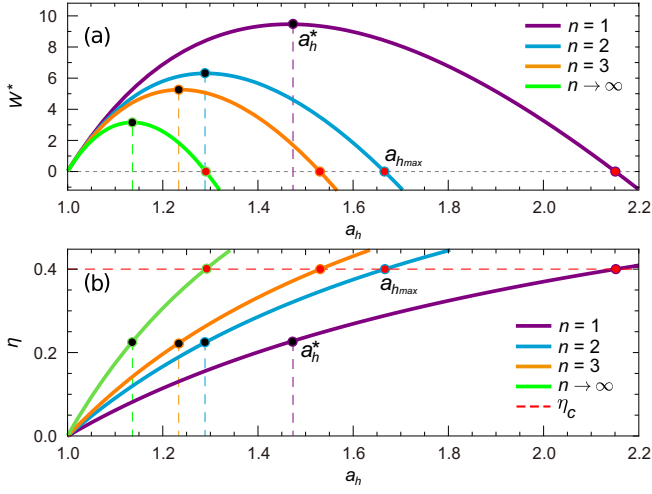


FIG. 3. (a) Work W^* vs. potential radius a_h curves for each $n = 1, 2, 3$ and $n \rightarrow \infty$ and (b) efficiency η vs. potential radius a_h together with the Carnot efficiency (red dashed) as comparison. The Figure is the result of an operating cycle in quasi-static state with 60,000 bosons wholly at non-condensed phase. The black dot indicates the efficiency at maximum work for corresponding n , whereas the red dot represents the $a_{h,max}$ as the maximum radius permitted. Each parameters are $T_h = 500$ nK, $T_l = 300$ nK, and $a_l = 1$

is when $T \geq T_c$ and Figure 4 represent numerical solutions of quasi-static Otto cycle which operated in condensed phase (BEC phase) that is when $T \leq T_c$. In this simulation parameters T_h (hot reservoir temperature), T_l (cold reservoir temperature) and a_l (initial potential radius) are kept constant, whilst a_h (final potential radius) is varied.

Figure 3 displays work and efficiency for several values of n for medium in non-condensed phase. Left shows the work curve versus a_h , and at each curve the maximum work is marked with a small black dot. For medium in non-condensed phase T_l and T_h are given equally for all n that is $T_l = 300$ nK and $T_h = 500$ nK. This is intended so that a comparison can be obtained. Right displays the efficiency curve versus a_h together with Carnot efficiency (η_c) at a constant value of $\eta = 0, 4$. a_h at maximum work is also shown in this efficiency curve which is denoted by efficiency at maximum work.

By obtaining the analytical solutions of total work in a cycle, we use Equation 12, which the first line is the solution for condensed phase and the second line is the solution for non-condensed phase. The total work for non-condensed phase is written as

$$W_{t_{con}} = bA'k_B^{b+1}a_l^3 \left(1 - \kappa^{\frac{1}{b}}\right) \times \left[T_h^{b+1}g_{b+1}(z_3) - \kappa^{-\frac{b+1}{b}}T_l^{b+1}g_{b+1}(z_2) \right] \quad (26)$$

z_2 and z_3 are the fugacity for point 2 and 3 respectively. Since during isentropic stroke there is no heat exchange from medium to the environment, the number of atoms N is fixed [42]. As a consequence Equation

9 must be constant during this process. By substituting the Temperature and Volume relation from Equation 25, we found fugacity must be constant during isentropic stroke, that is we have $z_1(a_h, T_1) = z_2(a_l, T_2)$ and $z_3(a_l, T_3) = z_4(a_h, T_4)$. Furthermore, at high temperature limit, we only need the first term of the expansion of Equation 7 because we obtain $\frac{N}{A'a^3(k_B T)^b} \ll 1$ by substituting an appropriate value of T . Therefore, Equation 26 is transformed to classical formulation of

$$W_t = bNk_B \left(1 - \kappa^{\frac{1}{b}}\right) \left[T_h - \kappa^{-\frac{1}{b}}T_l \right] \quad (27)$$

For fixed T_h and T_l value, the total work decreases as n increases, as shown in Figure 3. These results are in agreement with [70], which at constant external energy ϵ_0 whilst volume is varied, the total work produced in a cycle decreases with increasing degree of potential n .

In general, the efficiency of Equation 23 can be expressed as

$$\eta = 1 - \kappa^{\frac{1}{b}} \quad (28)$$

Furthermore, efficiency increases with increasing n , from Figure 3 we see that for small compression, (small a_h), engines operating at high n are more efficient than en-

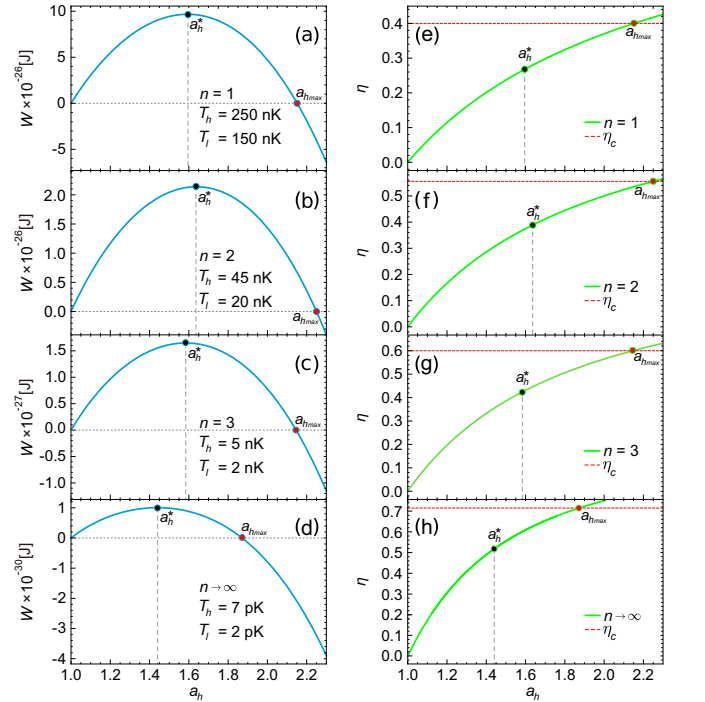


FIG. 4. The result of an operating cycle in quasi-static manner with 60,000 bosons wholly at condensed phase. The LHS column, (a)–(d), shows total work as a function of a_h , whilst the RHS column, (e)–(h), displays the curve of efficiency versus a_h along with Carnot efficiency (red-dashed) for each $n = 1, 2, 3$ and $n \rightarrow \infty$ respectively. The black dot and the red dot represent the same meaning as in Figure 3. In this simulation, both work and efficiency use the same T_h and T_l ; we set different T_h and T_l for each n correspond to the T_c on Table I.

gines operating at small n . These results are also consistent with those obtained in references [70].

Efficiency at maximum work is equal for all n , which is exactly Curzon-Ahlborn efficiency [39]. By deriving equation 27 with respect to κ , we get $\kappa_{max}^{\frac{1}{b}} = (T_l/T_h)^{\frac{1}{2}}$ so $\eta = 1 - (T_l/T_h)^{\frac{1}{2}}$. On Section IV B, we also see that efficiency at maximum power for medium in non-condensed phase is also equivalent to Curzon-Ahlborn efficiency.

In Figure 4 we represent the total work for several n for medium in condensed phase. T_l and T_h are chosen in such a way for each n medium is always below critical temperature. Need to be noted that for each n , we cannot display them in one figure as we did in Figure 3, this is due to the difference in critical temperature at each n . We get the analytical expression for total work for medium in condensed phase below

$$W_{t_{con}} = bA'k_B^{b+1}a_l^3 \left(1 - \kappa^{\frac{1}{b}}\right) \zeta(b+1) \times \left[T_h^{b+1} - \kappa^{-\frac{b+1}{b}}T_l^{b+1}\right] \quad (29)$$

$\zeta(b+1)$ is a zeta function originated from Equation 7, i.e. when $z = 1$. By dint of choosing the decreasing temperature as n increases, the maximum work obtained is also decreased as n increases as shown in Figure 4. But unlike in the non-condensed phase, where the optimum efficiency is the same for all n , the efficiency at the maximum work increases with increasing n . It shows that the optimum efficiency for medium in condensed phase is dependent on the properties of the medium.

In Section IV B, it is clearly seen that the efficiency at maximum power for medium in condensed phase is higher than Curzon-Ahlborn efficiency. Need to be noted that work in condensed phase is not explicitly a function of N (number of particles) because the number of condensed bosons is a function of temperature. Referring to Equation 9, we obtain the fraction of excited boson to total N ($T \leq T_c$) as written

$$\frac{N_T}{N} = \left(\frac{T}{T_c}\right)^b \quad (30)$$

The maximum excitation occurs when $T = T_c$ whilst minimum excitation occurs when all bosons are condensed, viz. when $T = 0$.

To obtain the ideal compression ratio (W is maximized), the Equation 29 is derived by κ

$$T_l^{b+1} \left[(b+1) - (b\kappa^*)^{\frac{1}{b}} \right] - T_h^{b+1} (\kappa^*)^{\frac{2+b}{b}} = 0 \quad (31)$$

κ^* and a^* are compression ratio and radius of potential at maximum work, respectively. The ideal κ^* and a^* for any number of n can be derived by solving the Equation 31 which the values are displayed in table II.

Based on the Table, the values do not change constantly as the variation of n is increased. It is due to the total work done in the shape of a sphere ($n = 2$) being equally distributed. Thus, the compression ratio

TABLE II. The engine parameters at non-condensed and condensed phase according to Figure 3 and 4, respectively.

n	<i>non - condensed</i>		<i>condensed</i>		κ^*
	a_h^*	$a_{h,max}$	a_h^*	$a_{h,max}$	
1	1,47	2,17	1,59	2,16	0,24
2	1,29	1,65	1,63	2,25	0,22
3	1,23	1,53	1,58	2,15	0,25
∞	1,13	1,28	1,44	1,82	0,33

required is lesser than other shapes. Because we are not really interested in engine that operates quasi-statically, due to long and infinite stroke time the power it produces is small to zero. We are more interested in finite time Otto cycle. The contact between medium and reservoir during the isochoric stroke is finite, medium is not in equilibrium with the thermal reservoir. But still during expansion and compression isentropic stroke are slow and quasi-static.

B. Endoreversible Performance

First of all, we review the efficiency and power output at condensed phase when the medium is under critical temperature. By substituting Equation 13, 17, and 21 to Equation 23, we derived similar efficiency as the quasi-static condition:

$$\eta_{T \leq T_c} = 1 - \kappa^{\frac{1}{b}} \quad (32)$$

while the power output is derived by combining Equation 17 and 22 with Equation 24, so as by using the relation of temperature in Equation 16, 21, and 25. As a result, the power output of condensed phase can be written below

$$P_{T \leq T_c} = \frac{bA'k_B^{b+1}g_{b+1}(1)a_l^3 \left(1 - \kappa^{\frac{1}{b}}\right) \left[\left[T_h \kappa^{\frac{1}{b}} e^{\alpha_l \tau_l} (e^{\alpha_h \tau_h} - 1) + T_l (e^{\alpha_l \tau_l} - 1) \right]^{b+1} - \left[T_l e^{\alpha_h \tau_h} (e^{\alpha_l \tau_l} - 1) + T_h \kappa^{\frac{1}{b}} (e^{\alpha_h \tau_h} - 1) \right]^{b+1} \right]}{\gamma(\tau_c + \tau_h) \kappa^{\frac{b+1}{b}} (e^{\alpha_h \tau_h + \alpha_c \tau_c} - 1)^{b+1}} \quad (33)$$

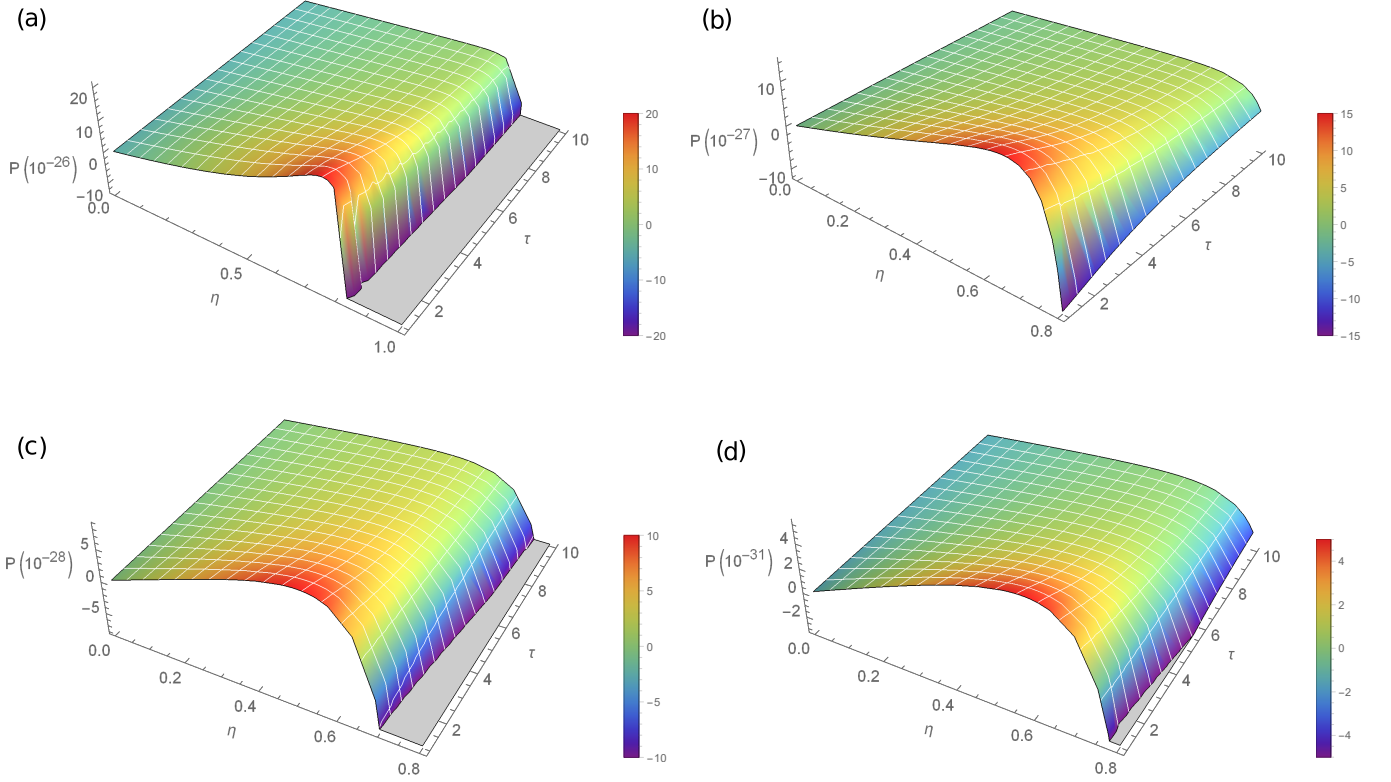


FIG. 5. 3D plot of power as function of η and τ for medium in BEC phase for (a) $n = 1$, (b) $n = 2$, (c) $n = 3$, and (d) $n \rightarrow \infty$, with hot and cold reservoir temperatures used are $T_h = 300$ nK and $T_l = 50$ nK, $T_h = 45$ nK and $T_l = 10$ nK, $T_h = 6$ nK and $T_l = 2$ nK, as well as $T_h = 8$ pK and $T_l = 2$ pK, respectively. The parameters are $\alpha_l = \alpha_h = \gamma = 1$.

which each T_h and T_l are the hot and cold reservoir temperatures, respectively, while each α_h and α_l represent the thermal conductivity while making contact with hot and cold reservoir, and the time of strokes within the heating and cooling process are denoted with τ_h and τ_l .

Furthermore, we obtain the efficiency of the non-condensed phase is the same as condensed phase, i.e.

$$\eta_{T \geq T_c} = 1 - \kappa^{\frac{1}{b}}. \quad (34)$$

Since efficiency is determined by the rate of work done during expansion and compression, for endoreversible cycle expansion and compression stroke is operated by isen-

tropic condition means its quasistatic, so there is no internal friction arises which will reduce efficiency [71]. However, the power output will be nonzero since the finite time process at isochoric stroke. This result indicates that in both quasi-static and endoreversible cases has no impact on engine efficiency but does on power. As obtained in the formulation of quasi-static work (Equation 26), the fugacity of Equation 7 is approximated only at the first term because the z value is small. T_3 and T_2 is derived from Equation 16, 21, and 25 so that the obtained power output is explicitly depend on N

$$P_{T \geq T_c} = \frac{bNk_B \left(1 - \kappa^{\frac{1}{b}}\right) \left[\left[T_h \kappa^{\frac{1}{b}} e^{\alpha_l \tau_l} (e^{\alpha_h \tau_h} - 1) + T_l (e^{\alpha_l \tau_l} - 1) \right] - \left[T_l e^{\alpha_h \tau_h} (e^{\alpha_l \tau_l} - 1) + T_h \kappa^{\frac{1}{b}} (e^{\alpha_h \tau_h} - 1) \right] \right]}{\gamma(\tau_c + \tau_h) \kappa^{\frac{1}{b}} (e^{\alpha_h \tau_h + \alpha_c \tau_c} - 1)} \quad (35)$$

need to be noted, at $T \geq T_c$, all bosons are in non-condensed phase and there is no condensed boson yet.

In contrast, at $T \leq T_c$, the amount of condensed boson depends on temperature so that N can not be written

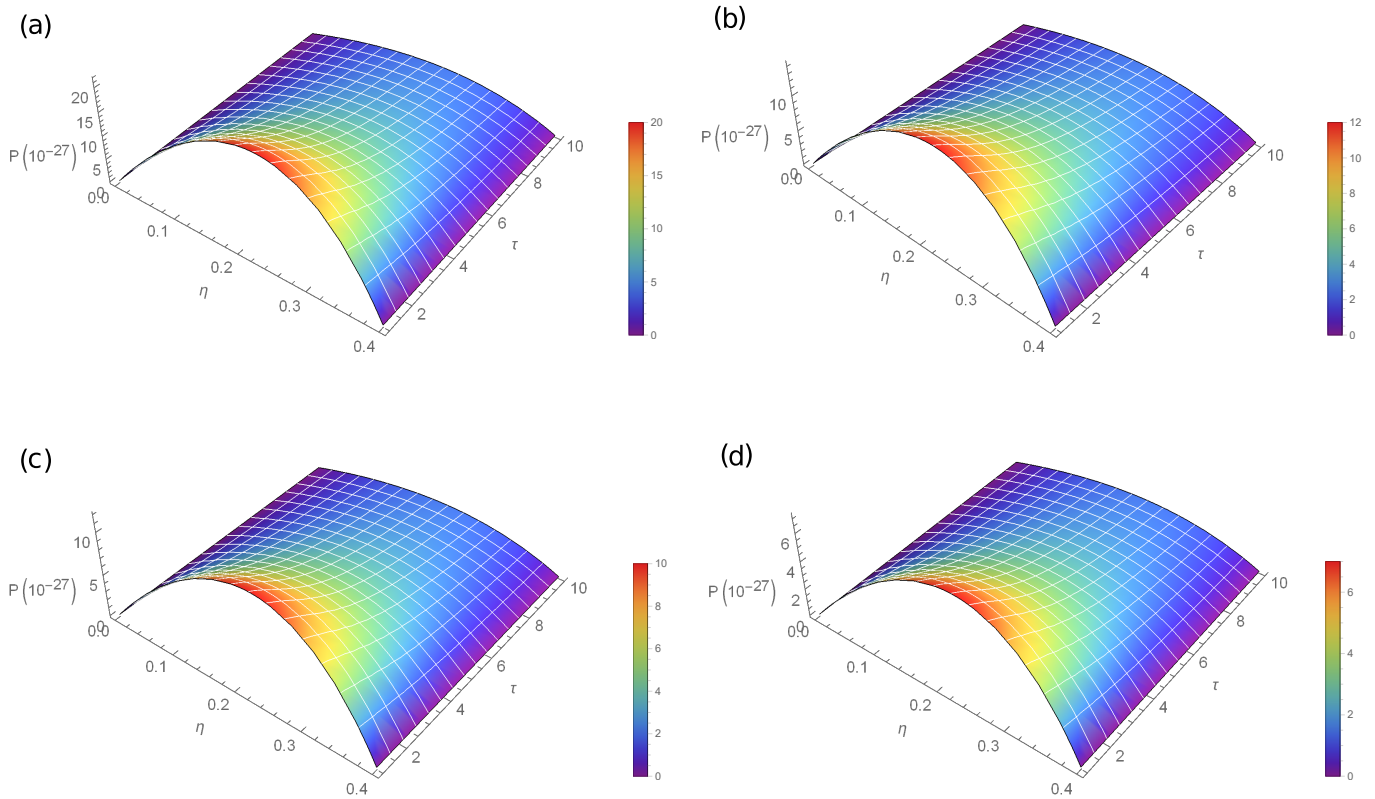


FIG. 6. 3D plot of power as function of η and τ for medium in non-condensed phase for (a) $n = 1$, (b) $n = 2$, (c) $n = 3$, and (d) $n \rightarrow \infty$, respectively. Cold and hot reservoir temperatures are 300 nK and 500 nK for all n . Other parameters are $\alpha_l = \alpha_h = \gamma = 1$.

explicitly. By replacing $\kappa^{\frac{1}{b}}$ with $1 - \eta$, power can also be represented as a function of efficiency. We visualize power as a function of efficiency (η) and isochoric stroke time (τ) by a 3D plot in Figure 5 for medium in BEC phase and in Figure 6 for medium in non-BEC phase.

We found that longer stroke times minimize power. This is due to the dependence of the denominator of the equation 33 on stroke time. Power is also minimized as efficiency approaches 1; it shows that engine performance is not only seen from its efficiency but also from the amount of power produced. By the reason of that, it is interesting to know at which efficiency the power becomes maximum. Efficiency at maximum power (EMP) is marked with a peak on each curve. The apex of this curve shifts to the left as τ increases, which means that EMP also decreases as τ increases. However, at high n the peak shift of the curve is small, so the increasing of τ does not have a significant effect on the decreasing of EMP.

We used T_h and T_l in this non-condensed phase slightly higher than the critical temperature of $n = 1$, so that none of the n has condensed. We also use this value in representing EMP in Figure 7. Although the shape of the curves are similar for all n , the power P decreases with the increasing of n , which is also confirmed by Figure 3a.

Unlike the power in the BEC phase where the peak of the curve shifts slightly with an increasing of τ , in non-condensed phase, the peak of the curve does not change with increasing of τ . This shows that the efficiency at maximum power of non-condensed phase does not depend on τ . As has been found in the quasi-static results, the efficiency at maximum power for the medium in the non-condensed phase is the Curzon-Ahlborn efficiency which only depends on the temperature of the reservoir. Curzon-Ahlborn efficiency is given by $\eta = 1 - (T_l/T_h)^{\frac{1}{2}}$ so we get $\eta = 0.22$ as exactly shown in Figure 6. The optimum efficiency achieved in the non-condensed phase is also lower than in the BEC phase.

It is well established that there is an inherent trade-off between efficiency and power [72]. Efficiency is maximized at long and infinite stroke time, but power is minimized for long stroke time due to dependence of the denominator in Equations 33 and 35. The highest efficiency is bounded by Carnot efficiency, that is when $\kappa^{\frac{1}{b}} = T_l/T_h$. By substituting this to Equation 33 or 35, we found that both in condensed phase and in non-condensed phase, power vanishes at that value. So it is important to find an optimum efficiency, Efficiency at Maximum Power (EMP). Similar to what Curzon and Ahlborn [39] did, then followed by many researchers [36, 42, 43, 67, 73–

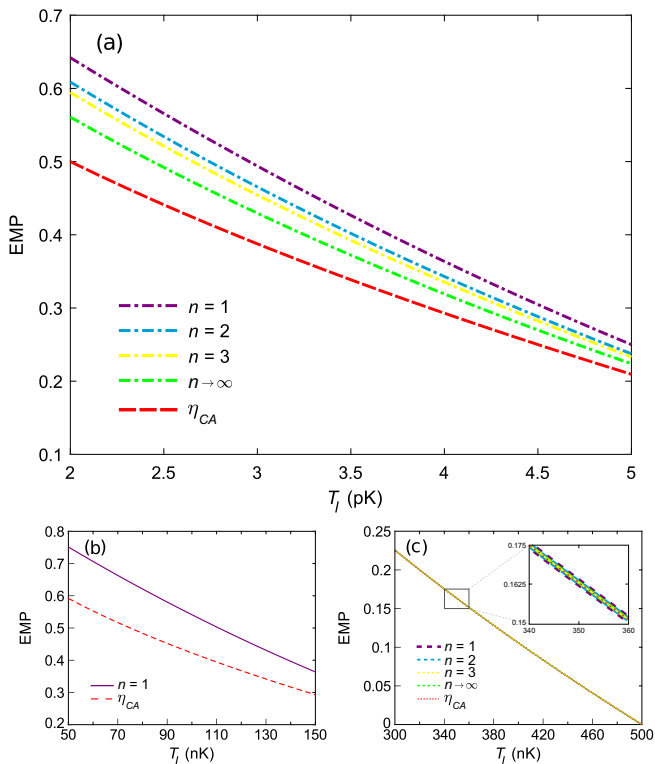


FIG. 7. (a) EMP vs T_l for medium in BEC phase for all n , using $T_h = 8$ pK. (b) EMP vs T_l for medium in condensed phase for $n = 1$, using $T_h = 300$ nK. (c) EMP for medium in non-condensed phase for all n , using $T_h = 500$ nK. On each curve, Curzon-Ahlborn efficiency (dashed red line) is given as a comparison. Others parameter are $\tau_l = \tau_h = \alpha_l = \alpha_h = \gamma = 1$.

75], we also determine EMP by maximizing Equations 33 and 35 with respect to κ , then the results are substituted back to Equations 32 and 34, which shown in Figure 7.

Since the critical temperature of $n \rightarrow \infty$ is the lowest, we used T_h and T_l which are comparable to the critical temperature of $n \rightarrow \infty$, thus all n is in the condensation phase. As shown in Figure 7a, EMP decreases as increasing of n and temperature of cold reservoir T_l , but still higher than Curzon-Ahlborn efficiency. Because of work in a quantum system is manifested by the difference between the initial and final energies of the system [76], this result can be linked to the change in internal energy during expansion and compression. Based on equation 12, the internal energy depends on the order of $(1/n)$, so $n = 1$ gives the highest expression of internal energy, and it reduces with the increasing of n . The power and EMP are inversely proportional to n . Moreover, EMP also shifts to Curzon-Ahlborn efficiency as the temperature of cold reservoir T_l increases, which can be seen in Figure 7b and Figure 7c.

Furthermore, although at $n = 1$ the highest EMP is produced, the power generated at picokelvin range is the lowest because P depends on the power of $b + 1$ (see

Equation 12). In addition, $n = 1$ has the largest b while $T \ll 1$, so the power generated is also very small. Therefore, we present the EMP for $n = 1$ separately in Figure 7b in nanokelvin range. In that case, we use $T_h = 300$ nK, slightly higher than its critical temperature, which resulting much higher power than in picokelvin range. Classically, work is produced from the movement of the piston when pressure is applied [42], but the atoms in the condensation phase cannot accept or use the pressure exerted on it [62]. Nevertheless, [42] claimed that work must be generated by the fraction of bosons out of condensate in the thermal cloud. At $n = 1$, the picokelvin temperature is very far below its critical temperature (see Equation 30), and almost all of the bosons have condensed, which causes only a few to be in the thermal cloud. Meanwhile, in the nanokelvin temperature range, which is slightly below its critical temperature, bosons are just starting to condense which causes some of them to still be in the thermal cloud. For this reason, the work and power generated in the nanokelvin range will be greater than the picokelvin range; this is as shown in Figure 7, the EMP in Figure 7b is higher than in Figure 7a.

At non-condensed phase, we obtained the optimal compression ratio as $\kappa_{max} = (T_l/T_h)^{b/2}$. By substituting it into Equation 34, we get $\eta = 1 - (T_l/T_h)^{1/2}$ in which is Curzon-Ahlborn efficiency. As shown in Figure 7c, EMP has the same value for all n . As we did previously, at high temperature limit, we took $\frac{N}{A'a^3} \ll 1$ where the term $\frac{N}{A'a^3}$ is the quantum property of bosons in a certain potential with the dimensions of energy. If $(k_B T)^b$ is much greater than $\frac{N}{A'a^3}$, then the quantum property of the gas can be neglected. Therefore, the energy of the bosons which was initially discrete has become continuous. When the energy of system matches classical conditions, the efficiency at maximum power is equal to the Curzon-Ahlborn efficiency [41]. However, when $\frac{N}{A'a^3}$ is comparable or greater than $(k_B T)^b$, the quantum effect of the gas cannot be neglected. Hence, the EMP also depends on a quantum property of the gas, including potential. Each potential gives different energy eigenvalue [77], so that it will affect the performance of the engine. Not only the difference in energy quantization affects performance, but in this study, we also found that the variations in the thermal contact time with the reservoir during isochoric strokes also affect the performance, especially the EMP. We visualize EMP for working medium in BEC phase as a function of cold bath temperature with different heating and cooling stroke time, τ_h and τ_l respectively. In this case, we only represented EMP in BEC phase since in non-condensation phase EMP is independent of heating and cooling stroke time.

In Figure 8a, we consider the engine works in an equal heating and cooling stroke time, $\tau_l = \tau_h$, which are varied in time units for all n . On the other hand, in Figure 8b, the heating and cooling stroke time are distinguished for only $n = 1$, the highest EMP producer, whereas all other parameters are kept constant. As seen in Figure 8a, the

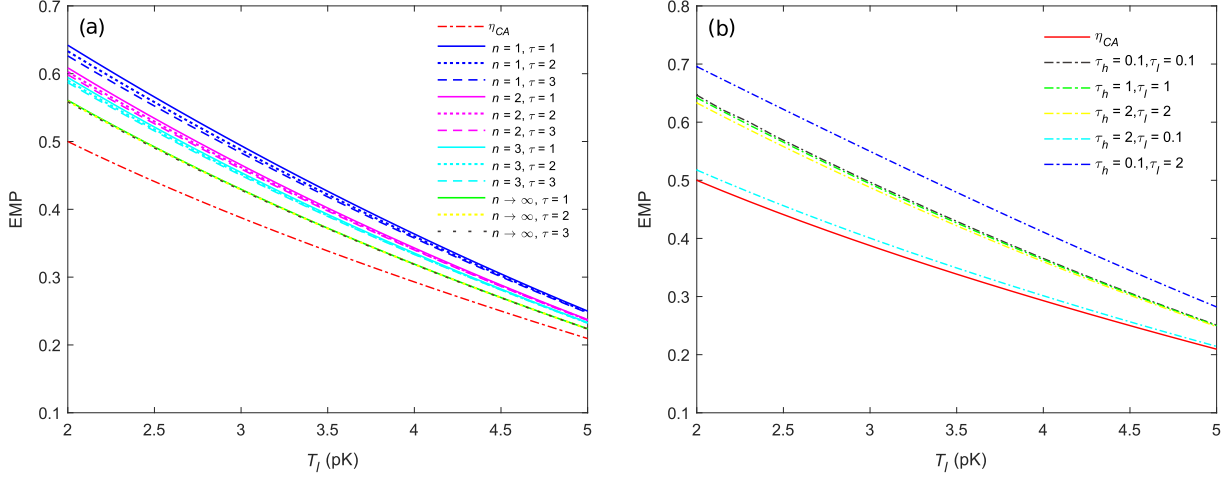


FIG. 8. EMP at BEC phase with variation in isochoric stroke time. (a) For all n with heating and cooling time equated, the solid line represents $\tau = 1$, dotted line represents $\tau = 2$, and dashed line represents $\tau = 3$. (b) For only $n = 1$ with heating and cooling stroke time is differentiated. For comparison in each curve Curzon-Ahlborn efficiency (η_{CA}) is also given. In both simulation we consider $T_h = 8$ pK while other parameters are $\alpha_l = \alpha_h = \gamma = 1$.

increasing of stroke time relatively decreases EMP even though at higher n does not give a significant difference. This result is not the same as obtained in prior research [42] in which the increasing of stroke time precisely increases the EMP produced. Ideally, the longer the stroke time makes the engine more likely reversible, and the engine that can exhibit reversibility would provide the highest efficiency [65]. However, there are also some interesting things we found in this study. Figure 8b shows that the EMP produced is significantly higher at short heating stroke time and long cooling stroke time. Otherwise, at long heating stroke time and a short cooling stroke time, the EMP produced is lower than other configurations even so close to Curzon-Ahlborn efficiency. Furthermore, EMP at $\tau_h < \tau_l$ is higher than EMP at $\tau_h = \tau_l$. Physically, it is due to the medium extracting more energy from hot reservoir when the heating stroke time is long, so that the temperature of medium reaches the temperature of hot reservoir itself. In contrast, during the short heating and long cooling stroke time, the medium ejects more energy into the cold reservoir so that the temperature drops. This is in agreement with Figure 7 that EMP is high at lower temperature and likewise.

The increasing efficiency at short and finite heating stroke time is known as the effect of residual coherence due to incomplete thermalizations [78]. In order to obtain a higher amount of power output, the cycle time should be cut down. At least there are two ways we can do this; first, by cutting the time during the expansion and compression strokes (shortcut to adiabaticity) [19, 71, 79, 80], and second by cutting the contact thermal time between the medium and the reservoir [78, 81, 82]. Nevertheless, in this study, we use an endoreversible cycle with the expansion and compression processes done in isentropic, i.e. quasi-static, so that we can only cut the time from

isochoric processes. Furthermore, due to rapid compression and expansion, internal friction (quantum friction) arises and directly reduces efficiency [71]. Finite-time transformation also exhibits entropy production, which leads the engine to irreversibility [65]. However, this irreversibility does not only occur during expansion and compression strokes but also in the heating and cooling strokes. Due to the short heating and cooling stroke time, the medium never reaches thermal equilibrium with the reservoir, thereby leaving the medium in a coherent state in the energy basis $|E_n\rangle$, or it is known as residual coherence. The coherence in this energy basis can be associated with entropy production and quantum friction [81]. Longer heating stroke time increases entropy production because it makes more heat flow from the hot reservoir to the medium. Mathematically, entropy is the amount of heat that flows for the increasing of every one degree in temperature [83], so that the longer the contact time of the medium to the hot reservoir, the higher entropy increases. The flowing heat does not occur continuously due to a thermal equilibrium will be achieved at a certain temperature that the entropy will not increase anymore.

Entropy production is closely related to the irreversibility of the engine [84]. The greater the entropy production, the more irreversible the engine becomes, leading to a decrease in efficiency at maximum power [81]. Here, we visualize the entropy production by investigating the entropy change during the heating and cooling process. By deriving Eq. 11 and utilizing the relations in Eqs. 16, 21, and 25, we obtained the entropy change in the heating process as follows

$$\Delta S_{heating} = (b+1)A'a_l^3 k_B^{b+1} \zeta(b+1) \times \left[[T_h + (T_2 - T_h) e^{-\alpha_h \tau_h}]^b - T_2^b \right] \quad (36)$$

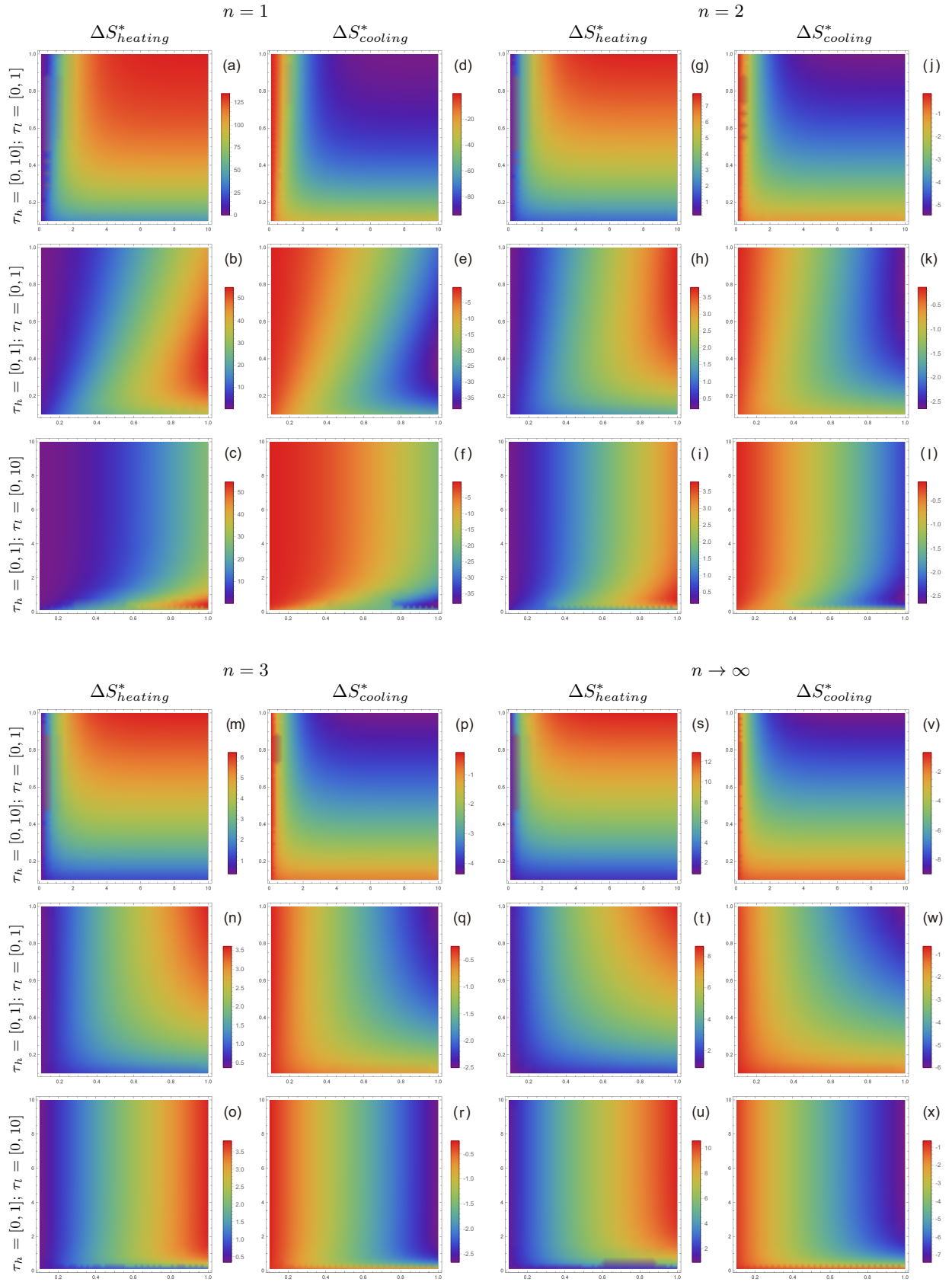


FIG. 9. The entropy change in heating (Eq. 37) and cooling (Eq. 40) process as a function of τ_h (x -axis) and τ_l (y -axis), with the temperatures T_h and T_l correspond to the interesting values in Figure 5 with the same parameter for each n .

which can be written in the form

$$\Delta S_{heating}^* = [T_h + (T_2 - T_h) e^{-\alpha_h \tau_h}]^b - T_2^b \quad (37)$$

with $\Delta S_{heating}^* = \Delta S_{heating}/C$, whereas

$$T_2 = \frac{T_l e^{\alpha_h \tau_h} (e^{\alpha_l \tau_l} - 1) + T_h \kappa^{\frac{1}{b}} (e^{\alpha_h \tau_h} - 1)}{\kappa^{\frac{1}{b}} (e^{\alpha_l \tau_l + \alpha_h \tau_h} - 1)} \quad (38)$$

Meanwhile, the entropy change within the cooling process is described as

$$\Delta S_{cooling} = (b+1) A' a_h^3 k_B^{b+1} \zeta(b+1) \times [[T_l + (T_4 - T_l) e^{-\alpha_l \tau_l}]^b - T_4^b] \quad (39)$$

with a similar idea, we rewrite the Eq. 39 in the form

$$\Delta S_{cooling}^* = [T_l + (T_4 - T_l) e^{-\alpha_l \tau_l}]^b - T_4^b \quad (40)$$

while

$$T_4 = \frac{T_l (e^{\alpha_l \tau_l} - 1) + T_h \kappa^{\frac{1}{b}} (e^{\alpha_h \tau_h} - 1) e^{\alpha_l \tau_l}}{e^{\alpha_l \tau_l + \alpha_h \tau_h} - 1} \quad (41)$$

In the cooling process, heat is transferred from the medium to the cold reservoir, so the change in entropy is negative. In finite time cycles such as endoreversible cycles, the entropy production during heating and cooling does not cancel each other or $\Delta S_{heating} + \Delta S_{cooling} > 0$, as shown in Figure 9. The amount of heat flow during heating stroke is not the same as the amount of heat flow during cooling stroke. Only reversible engines, such as Carnot engine, produce zero entropy during the cycle [81]. Thus, the efficiency of an irreversible engine will never reach Carnot's efficiency. However, this entropy production could be minimized by reducing the amount of heat transferred to the medium or reducing the heating stroke time. According to Figure 9c, the entropy of heating process is relatively lower compared to Figures 9a and 9b; this result is noticed obviously by the presence of the color more "blue". These results are also in agreement with the results obtained in Figure 8b, in which EMP is relatively higher when the heating time τ_h is shortened.

Moreover, based on Figure 8b, both τ_l and τ_h are actually affected EMP. It can be seen that the blue and black dashes work at the same τ_h , but EMP is higher at shorten τ_h . Physically, the temperature of medium in blue dash is lower than temperature in black dash because more heat is injected from medium into the cold reservoir. In BEC, the fraction of condensed atoms depends on temperature (Eq. 9), the fraction of bosons condensed on the blue dash will be larger than on the black dash. When condensations are formed, these bosons will be occupied to the lowest quantum state or, macroscopically, the wave properties of each atom will collapse and interfere constructively with each other and form a single wave function [85]. This coherence effect arises from the

occupation of atoms in the condensate in the same quantum state, which is described by the single wave function [86]. Based on this fact, blue will be "more coherent" than black. The increasing coherence in the boson state emerges when an incomplete thermalization process occurs, particularly when $\tau_h < \tau_l$, which leads to the reduction in entropy production (see Figure 9c). Thus, it can be said that the presence of this coherence due to incomplete thermalization contributes to an elevation in EMP [81]. On the other hand, when $\tau_h > \tau_l$, this process does not guarantee an increase in coherence and a reduction in entropy. Therefore, we gain a specific case to enhance the EMP only when incomplete thermalization occurs at $\tau_h < \tau_l$ (see Figure 8b).

The study shows EMP is higher when using BEC as a working medium than normal boson gas (non-condensed conditions). The best performance is also given by the potential with $n = 1$ because it produces the highest power and EMP. In addition, its critical temperature is relatively easy to reach and close to the temperature of experimental realizations of BEC itself [87]. Nevertheless, the power generated by $n = 1$ is still very small when compared to the real engine due to the engine operating at very low temperatures even though the efficiency of using BEC is much higher than the efficiency provided by classical gas [36, 39, 47, 48]. Since the power is determined by changes in internal energy during expansion and compression, it is possible to boost the power by adding more particles or by increasing external potential ϵ_0 (in this calculation, we used ϵ_0 corresponding to prior study [42]). However, increasing the number of particles will increase the density of the gas, so the interaction between atoms in gas cannot be neglected. Moreover, based on experimental results, BEC only occurs at very low densities [56, 57, 88]. The critical temperature also depends on particle density, the rise in density also rising T_c which is relatively easy to access [69]. It is necessary to consider other physical aspects such as the volume of the potential as shown in Equation 1 so that BEC can still occur.

V. CONCLUSION

Bose-Einstein Condensation (BEC) is one of the matters which can be harnessed as a working medium in the QHE idea. Here, we focus on investigating EMP using BEC trapped in a generalized external potential instead of the non-BEC because of its dependent on medium properties and external potential. At the same range of T , for various degrees of potential n , EMP decreases as n increases, whilst η increases as n increases. Moreover, we also investigate the EMP in BEC regimes by varying isochoric stroke times (τ_l and τ_h). Both τ_l and τ_h directly affect the final temperatures of the medium in each isochoric stroke through the Fourier Conduction Law (T_1 and T_3) (see Equation 21). Despite the fact that EMP is decreasing for a longer stroke time, there is no significant

difference for the same value of τ_l and τ_h . However, if we set τ_l and τ_h properly, e.g., short stroke time in the heating isochoric process and long stroke time in the cooling isochoric process, the engine produces higher EMP than the one operates in long heating stroke time and short cooling stroke time, surprisingly also higher than operates in equal heating and cooling stroke time. This indicates that the setting of the stroke time of the engine can restrain the entropy production as well as quantum friction in the system. When the entropy change in the heating process exceeds the entropy in the cooling process, resulting in a positive ΔS , residual coherence emerges due to incomplete thermalization. Furthermore, with the uniqueness of the BEC regime, the optimal work extracted can be obtained within the full excited expansion stroke, (the closest by T_C), and full condensed compression stroke, (the farthest by T_C). Hence, we conclude that the quantum Otto engine operates more effectively on potential $n = 1$ than other variations of n whose the highest critical temperature, so as being the

highest EMP and highest power output producer. In-depth exploration for further study involves examining the interaction between the number of particles and the specific parameter ϵ_0 with the external potential. Additionally, gaining a comprehensive insight into the interactions between bosonic particles significantly enhances our understanding, unveiling a more realistic behavior of these particles, especially under high-density conditions. These investigations hold paramount importance in the development of a genuinely realistic nano-engine, providing deeper insights into the dependencies governing its performance.

ACKNOWLEDGMENTS

TEPS thanks the Faculty of Mathematics and Natural Sciences, Andalas University, for financially supporting this research with research grant No. 04/UN.16.03.D/PP/FMIPA/2022.

-
- [1] S. Deffner and S. Campbell, *Quantum Thermodynamics*, 2053-2571 (Morgan & Claypool Publishers, 2019).
- [2] R. V. Chamberlin, The big world of nanothermodynamics, *Entropy* **17**, 52 (2015).
- [3] W. Dong, Nanoscale thermodynamics needs the concept of a disjoining chemical potential, *Nature Communications* **14**, 1824 (2023).
- [4] F. J. Peña, N. M. Myers, D. Órdenes, F. Albarrán-Arriagada, and P. Vargas, Enhanced efficiency at maximum power in a fock-darwin model quantum dot engine, *Entropy* **25**, 518 (2023).
- [5] O. Galteland, D. Bedeaux, and S. Kjelstrup, Nanothermodynamic description and molecular simulation of a single-phase fluid in a slit pore, *Nanomaterials* **11**, 165 (2021).
- [6] B. A. Strøm, J. He, D. Bedeaux, and S. Kjelstrup, When thermodynamic properties of adsorbed films depend on size: Fundamental theory and case study, *Nanomaterials* **10**, 1691 (2020).
- [7] R. de Miguel and J. M. Rubí, Statistical mechanics at strong coupling: A bridge between landsberg's energy levels and hill's nanothermodynamics, *Nanomaterials* **10**, 2471 (2020).
- [8] Y. Yin, L. Chen, and F. Wu, Performance of quantum stirling heat engine with numerous copies of extreme relativistic particles confined in 1d potential well, *Physica A: Statistical Mechanics and its Applications* **503**, 58 (2018).
- [9] B. A. Strøm, J.-M. Simon, S. K. Schnell, S. Kjelstrup, J. He, and D. Bedeaux, Size and shape effects on the thermodynamic properties of nanoscale volumes of water, *Phys. Chem. Chem. Phys.* **19**, 9016 (2017).
- [10] S. Kjelstrup, S. K. Schnell, T. J. H. Vlugt, J.-M. Simon, A. Bardow, D. Bedeaux, and T. Trinh, Bridging scales with thermodynamics: from nano to macro, *Advances in Natural Sciences: Nanoscience and Nanotechnology* **5**, 023002 (2014).
- [11] J. Kim, S.-h. Oh, D. Yang, J. Kim, M. Lee, and K. An, A photonic quantum engine driven by superradiance, *Nature Photonics* **16**, 707 (2022).
- [12] H. E. D. Scovil and E. O. Schulz-DuBois, Three-level masers as heat engines, *Phys. Rev. Lett.* **2**, 262 (1959).
- [13] M. Kim, M. Scully, and A. Svidzinsky, A supercharged photonic quantum heat engine, *Nature Photonics* **16**, 669 (2022).
- [14] N. M. Myers, O. Abah, and S. Deffner, Quantum thermodynamic devices: From theoretical proposals to experimental reality, *AVS Quantum Science* **4**, 027101 (2022).
- [15] H. T. Quan, Y.-x. Liu, C. P. Sun, and F. Nori, Quantum thermodynamic cycles and quantum heat engines, *Phys. Rev. E* **76**, 031105 (2007).
- [16] N. Papadatos, The quantum otto heat engine with a relativistically moving thermal bath, *International Journal of Theoretical Physics* **60**, 4210 (2021).
- [17] L. Li, H. Li, W. Yu, Y. Hao, L. Li, and J. Zou, Shortcut-to-adiabaticity quantum tripartite otto cycle, *Journal of Physics B: Atomic, Molecular and Optical Physics* **54**, 215501 (2021).
- [18] S. Singh and O. Abah, Energy optimization of two-level quantum otto machines (2020), arXiv:2008.05002 [cond-mat.stat-mech].
- [19] O. Abah and M. Paternostro, Shortcut-to-adiabaticity otto engine: A twist to finite-time thermodynamics, *Phys. Rev. E* **99**, 022110 (2019).
- [20] F. Altintas, Comparison of the coupled quantum carnot and otto cycles, *Physica A: Statistical Mechanics and its Applications* **523**, 40 (2019).
- [21] A. Fahriza, T. E. P. Sutantyo, and Z. Abdullah, Optimizations of multilevel quantum engine with n noninteracting fermions based on lenoir cycle, *The European Physical Journal Plus* **137**, 1030 (2022).
- [22] A. Fahriza and T. E. P. Sutantyo, *Jurnal Ilmu Fisika* **14**, 95-107 (2022).
- [23] F. Abdillah and Y. D. Saputra, Quantum-mechanical brayton engine based on a boson particle inside cubic

- potential, *Journal of Physics: Conference Series* **1726**, 012004 (2021).
- [24] Y. D. Saputra, Quantum lenoir engine with a multiple-eigenstates particle in 1d potential box, *Journal of Physics: Conference Series* **1726**, 012016 (2021).
- [25] M. H. Ahmadi, M. A. Nazari, and M. Feidt, Thermodynamic analysis and multi-objective optimisation of endoreversible lenoir heat engine cycle based on the thermo-economic performance criterion, *International Journal of Ambient Energy* **40**, 600 (2019).
- [26] R. Wang, J. Wang, J. He, and Y. Ma, Performance of a multilevel quantum heat engine of an ideal n -particle fermi system, *Phys. Rev. E* **86**, 021133 (2012).
- [27] S. Singh and S. Rebari, Multi-level quantum diesel engine of non-interacting fermions in a one-dimensional box, *The European Physical Journal B* **93**, 150 (2020).
- [28] D. P. Setyo, E. Latifah, A. Hidayat, and H. Wisodo, Quantum relativistic diesel engine with single massless fermion in 1 dimensional box system, *Jurnal Penelitian Fisika dan Aplikasinya (JPFA)* **8**, 25–32 (2018).
- [29] C. M. Bender, D. C. Brody, and B. K. Meister, Quantum mechanical carnot engine, *Journal of Physics A: Mathematical and General* **33**, 4427 (2000).
- [30] C. M. Bender, D. C. Brody, and B. K. Meister, Entropy and temperature of a quantum carnot engine, *Proceedings of the Royal Society of London. Series A: Mathematical, Physical and Engineering Sciences* **458**, 1519 (2002).
- [31] F. Moukalled, R. Y. Nuwayhid, and N. Noueihed, The efficiency of endoreversible heat engines with heat leak, *International Journal of Energy Research* **19**, 377 (1995).
- [32] I. H. Belfaqih, T. E. P. Sutanty, T. B. Prayitno, and A. Sulaksono, Quantum-carnot engine for particle confined to 2D symmetric potential well, *AIP Conference Proceedings* **1677**, 040010 (2015).
- [33] T. E. P. Sutanty, Three-state quantum heat engine based on carnot cycle, *Jurnal Fisika Unand* **9**, 142 (2020).
- [34] T. E. P. Sutanty, I. H. Belfaqih, and T. B. Prayitno, Quantum-carnot engine for particle confined to cubic potential, *AIP Conference Proceedings* **1677**, 040011 (2015).
- [35] M. O. Scully, M. S. Zubairy, G. S. Agarwal, and H. Walther, Extracting work from a single heat bath via vanishing quantum coherence, *Science* **299**, 862 (2003).
- [36] S. Deffner, Efficiency of harmonic quantum otto engines at maximal power, *Entropy* **20**, 875 (2018).
- [37] T. D. Kieu, Quantum heat engines, the second law and maxwell's daemon, *The European Physical Journal D - Atomic, Molecular, Optical and Plasma Physics* **39**, 115 (2006).
- [38] T. D. Kieu, The second law, maxwell's demon, and work derivable from quantum heat engines, *Phys. Rev. Lett.* **93**, 140403 (2004).
- [39] F. L. Curzon and B. Ahlborn, Efficiency of a carnot engine at maximum power output, *American Journal of Physics* **43**, 22 (1975).
- [40] O. Abah, J. Roßnagel, G. Jacob, S. Deffner, F. Schmidt-Kaler, K. Singer, and E. Lutz, Single-ion heat engine at maximum power, *Phys. Rev. Lett.* **109**, 203006 (2012).
- [41] R. Kosloff and Y. Rezek, The quantum harmonic otto cycle, *Entropy* **19**, 136 (2017).
- [42] N. M. Myers, F. J. Peña, O. Negrete, P. Vargas, G. D. Chiara, and S. Deffner, Boosting engine performance with bose-einstein condensation, *New Journal of Physics* **24**, 025001 (2022).
- [43] N. M. Myers and S. Deffner, Bosons outperform fermions: The thermodynamic advantage of symmetry, *Phys. Rev. E* **101**, 012110 (2020).
- [44] J. Roßnagel, O. Abah, F. Schmidt-Kaler, K. Singer, and E. Lutz, Nanoscale heat engine beyond the carnot limit, *Phys. Rev. Lett.* **112**, 030602 (2014).
- [45] Z. Smith, P. S. Pal, and S. Deffner, Endoreversible otto engines at maximal power, *Journal of Non-Equilibrium Thermodynamics* **45**, 305 (2020).
- [46] Z. Zettira, T. E. P. Sutanty, and Z. Abdullah, *Jurnal Ilmu Fisika* **16**, 22 (2024), (Forthcoming).
- [47] L. Erbay and H. Yavuz, Analysis of the stirling heat engine at maximum power conditions, *Energy* **22**, 645 (1997).
- [48] H. S. Leff, Thermal efficiency at maximum work output: New results for old heat engines, *American Journal of Physics* **55**, 602 (1987).
- [49] N. M. Myers, F. J. Peña, N. Cortés, and P. Vargas, Multilayer graphene as an endoreversible otto engine (2022), arXiv:2212.03286 [cond-mat.stat-mech].
- [50] O. Fialko and D. W. Hallwood, Isolated quantum heat engine, *Phys. Rev. Lett.* **108**, 085303 (2012).
- [51] M. Gluza, J. a. Sabino, N. H. Ng, G. Vitagliano, M. Pezzutto, Y. Omar, I. Mazets, M. Huber, J. Schmiedmayer, and J. Eisert, Quantum field thermal machines, *PRX Quantum* **2**, 030310 (2021).
- [52] J. Li, E. Y. Sherman, and A. Ruschhaupt, Quantum heat engine based on a spin-orbit- and zeeman-coupled bose-einstein condensate, *Phys. Rev. A* **106**, L030201 (2022).
- [53] J. Li, T. Fogarty, S. Campbell, X. Chen, and T. Busch, An efficient nonlinear feshbach engine, *New Journal of Physics* **20**, 015005 (2018).
- [54] A. Einstein, *Quantentheorie des einatomigen idealen Gases*, *Sitzungsberichte der Preussischen Akademie der Wissenschaften. Physikalisch-mathematische Klasse No. bk. 2* (Verlag d. Akad. d. Wiss., 1925).
- [55] Bose, Plancks gesetz und lichtquantenhypothese, *Zeitschrift für Physik* **26**, 178 (1924).
- [56] M. H. Anderson, J. R. Ensher, M. R. Matthews, C. E. Wieman, and E. A. Cornell, Observation of bose-einstein condensation in a dilute atomic vapor, in *Collected Papers of Carl Wieman* (World Scientific, 2008) pp. 453–456.
- [57] K. B. Davis, M. O. Mewes, M. R. Andrews, N. J. van Druten, D. S. Durfee, D. M. Kurn, and W. Ketterle, Bose-einstein condensation in a gas of sodium atoms, *Phys. Rev. Lett.* **75**, 3969 (1995).
- [58] C. C. Bradley, C. A. Sackett, and R. G. Hulet, Bose-einstein condensation of lithium: Observation of limited condensate number, *Phys. Rev. Lett.* **78**, 985 (1997).
- [59] C. C. Bradley, C. A. Sackett, J. J. Tollett, and R. G. Hulet, Evidence of bose-einstein condensation in an atomic gas with attractive interactions, *Phys. Rev. Lett.* **75**, 1687 (1995).
- [60] A. L. Gaunt, T. F. Schmidutz, I. Gotlibovych, R. P. Smith, and Z. Hadzibabic, Bose-einstein condensation of atoms in a uniform potential, *Phys. Rev. Lett.* **110**, 200406 (2013).
- [61] V. Bagnato, D. E. Pritchard, and D. Kleppner, Bose-einstein condensation in an external potential, *Phys. Rev. A* **35**, 4354 (1987).
- [62] R. Pathria and P. D. Beale, 15 - fluctuations and nonequilibrium statistical mechanics, in *Statistical Mechanics*, edited by R. Pathria and P. D. Beale (Academic Press,

- Boston, 2011) 3rd ed., pp. 583–635.
- [63] L. Pitaevskii and S. Stringari, *Bose-Einstein Condensation and Superfluidity* (Oxford University Press, New York, 2016).
- [64] K. Hoffmann, J. Burzler, and S. Schubert, Endoreversible thermodynamics, *Journal of Non-Equilibrium Thermodynamics* **22**, 311 (1997).
- [65] Y. A. Çengel and M. A. Boles, *Thermodynamics : An Engineering Approach*, 5th ed. (McGraw-Hill, New York, 2008).
- [66] J. Wang and J. He, Optimization on a three-level heat engine working with two noninteracting fermions in a one-dimensional box trap, *Journal of Applied Physics* **111**, 043505 (2012).
- [67] H. Wang, S. Liu, and J. He, Performance analysis and parametric optimum criteria of an irreversible bose–otto engine, *Journal of Applied Physics* **105**, 083534 (2009).
- [68] D. C. Aveline, J. R. Williams, E. R. Elliott, C. Dutenhofer, J. R. Kellogg, J. M. Kohel, N. E. Lay, K. Oudrhiri, R. F. Shotwell, N. Yu, and R. J. Thompson, Observation of bose–einstein condensates in an earth-orbiting research lab, *Nature* **582**, 193 (2020).
- [69] J. D. Reppy, B. C. Crooker, B. Hebral, A. D. Corwin, J. He, and G. M. Zassenhaus, Density dependence of the transition temperature in a homogeneous bose-einstein condensate, *Phys. Rev. Lett.* **84**, 2060 (2000).
- [70] Y. Zheng and D. Poletti, Work and efficiency of quantum otto cycles in power-law trapping potentials, *Phys. Rev. E* **90**, 012145 (2014).
- [71] S. Çakmak, F. Altintas, A. Gençten, and Ö. E. Müstecaplıoğlu, Irreversible work and internal friction in a quantum otto cycle of a single arbitrary spin, *The European Physical Journal D* **71**, 75 (2017).
- [72] S. Çakmak and Ö. E. Müstecaplıoğlu, Spin quantum heat engines with shortcuts to adiabaticity, *Phys. Rev. E* **99**, 032108 (2019).
- [73] J. Wang, Z. Wu, and J. He, Quantum otto engine of a two-level atom with single-mode fields, *Phys. Rev. E* **85**, 041148 (2012).
- [74] R. Wang, J. Wang, J. He, and Y. Ma, Efficiency at maximum power of a heat engine working with a two-level atomic system, *Phys. Rev. E* **87**, 042119 (2013).
- [75] Z. Smith, P. S. Pal, and S. Deffner, Endoreversible otto engines at maximal power, *Journal of Non-Equilibrium Thermodynamics* **45**, 305 (2020).
- [76] A. J. Roncaglia, F. Cerisola, and J. P. Paz, Work measurement as a generalized quantum measurement, *Phys. Rev. Lett.* **113**, 250601 (2014).
- [77] S. Mahajan, Quantum mechanics in power-law potentials, *American Journal of Physics* **88**, 431 (2020).
- [78] S. Chand, S. Dasgupta, and A. Biswas, Finite-time performance of a single-ion quantum otto engine, *Phys. Rev. E* **103**, 032144 (2021).
- [79] A. d. Campo, J. Goold, and M. Paternostro, More bang for your buck: Super-adiabatic quantum engines, *Scientific Reports* **4**, 6208 (2014).
- [80] A. del Campo, Shortcuts to adiabaticity by counterdiabatic driving, *Phys. Rev. Lett.* **111**, 100502 (2013).
- [81] P. A. Camati, J. F. G. Santos, and R. M. Serra, Coherence effects in the performance of the quantum otto heat engine, *Phys. Rev. A* **99**, 062103 (2019).
- [82] F. Plastina, A. Alecce, T. J. G. Apollaro, G. Falcone, G. Francica, F. Galve, N. Lo Gullo, and R. Zambrini, Irreversible work and inner friction in quantum thermodynamic processes, *Phys. Rev. Lett.* **113**, 260601 (2014).
- [83] D. V. Schroeder, *An introduction to thermal physics* (American Association of Physics Teachers, 1999).
- [84] T. Mihaescu and A. Isar, Irreversibility and entropy production in two coupled bosonic modes interacting with a thermal environment, *The European Physical Journal Plus* **139**, 82 (2024).
- [85] W. Ketterle and H.-J. Miesner, Coherence properties of bose-einstein condensates and atom lasers, *Phys. Rev. A* **56**, 3291 (1997).
- [86] E. A. Donley, N. R. Claussen, S. T. Thompson, and C. E. Wieman, Atom–molecule coherence in a bose–einstein condensate, *Nature* **417**, 529 (2002).
- [87] C. C. Bradley, C. A. Sackett, J. J. Tollett, and R. G. Hulet, Evidence of bose-einstein condensation in an atomic gas with attractive interactions, *Phys. Rev. Lett.* **75**, 1687 (1995).
- [88] A. Görlitz, J. M. Vogels, A. E. Leanhardt, C. Raman, T. L. Gustavson, J. R. Abo-Shaer, A. P. Chikkatur, S. Gupta, S. Inouye, T. Rosenband, and W. Ketterle, Realization of bose-einstein condensates in lower dimensions, *Phys. Rev. Lett.* **87**, 130402 (2001).